SANDIA REPORT

SAND99–8694
Unlimited Release
Printed November 1999

The Autocatalytic Behavior Of Trimethylindium During Thermal Decomposition

(Accepted for publication in *Chemistry of Materials,* October 29, 1999)

Anthony H. McDaniel, M. D. Allendorf

Prepared by
Sandia National Laboratories
Albuquerque, New Mexico 87185 and Livermore, California 94550

Sandia is a multiprogram laboratory operated by Sandia Corporation, a Lockheed Martin Company, for the United States Department of Energy under Contract DE-AC04-94AL85000.

Sandia National Laboratories

Issued by Sandia National Laboratories, operated for the United States Department of Energy by Sandia Corporation.

Available to DOE and DOE contractors from
Office of Scientific and Technical Information
P.O. Box 62
Oak Ridge, TN 37831

Prices available from (703) 605-6000
Web site: http://www.ntis.gov/ordering.htm

Available to the public from
National Technical Information Service
U.S. Department of Commerce
5285 Port Royal Rd
Springfield, VA 22161

NTIS price codes
Printed copy: A03
Microfiche copy: A01

DISCLAIMER

Portions of this document may be illegible in electronic image products. Images are produced from the best available original document.

SAND 99-8694

Unlimited Release

Printed November 1999

The Autocatalytic Behavior Of Trimethylindium During Thermal Decomposition

accepted for publication in Chemistry of Materials, October 29, 1999

Anthony H. McDaniel and Mark D. Allendorf

Combustion Research Facility

Sandia National Laboratories

Livermore, CA 94551

Abstract

Pyrolysis of trimethylindium (TMIn) in a hot-wall flow-tube reactor has been investigated at temperatures between 573 and 723 K using a modulated molecular-beam mass-sampling technique and detailed numerical modeling. The TMIn was exposed to various mixtures of carrier gases: He, H_2, D_2, and C_2H_4, in an effort to elucidate the behavior exhibited by this compound in different chemical environments. The decomposition of TMIn is a heterogeneous, autocatalytic process with an induction period that is carrier-gas dependent and lasts on the order of minutes. After activation of the tube wall, the thermolysis exhibits a steady-state behavior that is surface mediated. This result is contrary to prior literature reports, which state that decomposition occurs in the gas phase via successive loss of the CH_3 ligands. This finding also suggests that the bond dissociation energy for the $(CH_3)_2In\text{-}CH_3$ bond derived from flow-tube investigations is erroneous and should be reevaluated.

This page intentionally left blank

I. Introduction

Metalorganic chemical vapor deposition (MOCVD) is a key process in the manufacture of Group IIIA-VA advanced optoelectronic materials, such as ternary and quaternary multi-junction solar cells, photodiodes, photodetectors, and tunable diode lasers.[1-4] Of particular relevance to the MOCVD community is an understanding of the reactivity and thermal stability of the Group IIIA organometallic precursors, the most widely used of which are the trimethyl-alkyls of aluminum (TMAl), gallium (TMGa), and indium (TMIn).[2] For TMIn in particular, the currently held principles regarding thermal stability and mechanisms for decomposition date back to the seminal paper authored by Jacko and Price 35 years ago.[5] Few if any reports on this subject disagree with their original findings that the decomposition of TMIn is initiated by homolytic fission of the metal-carbon bond.

The early observations of Jacko and Price spawned several investigations into the energetics of the metal-carbon bond scission process for TMIn, with the majority of experimentalists using hot-wall flow-tube reactors to conduct their research.[6-8] These investigators endorsed two primary assumptions put forth by Jacko and Price: (1) the decomposition process in the flow reactor is entirely homogeneous and is initiated by the loss of the first methyl ligand,

$$In(CH_3)_3 \leftrightarrows In(CH_3)_2 + CH_3 \qquad [1]$$

and (2), below a certain temperature reaction [1] is rate limiting. As a result of these hypotheses, the bond dissociation energy (BDE) for the $(CH_3)_2In\text{-}CH_3$ bond has been equated to the activation energy for reaction [1] extracted from flow-reactor data,[9,10] thereby establishing the metric of thermal stability for TMIn.

Given the apparent simplicity of this chemical system, it is surprising to note the uncertainty that permeates the literature regarding reaction pathways and the energetics of bond scission. Since Jacko and Price published their results, there have been four reports documenting

a complex pyrolytic behavior that is dependent upon the carrier-gas composition.[6,7,11,12] Specifically, investigators have observed a slower rate of TMIn decomposition in inert carriers such as He or N_2 than in H_2. They have also reported the existence of surface deposits, either carbonaceous or metallic, within the flow tubes such that repeatable observations could only be achieved in *seasoned* vessels. These experimental anomalies result in an inconsistent determination of the activation energy for reaction [1], where values that range from 36 to 54 kcal mol^{-1} have been reported.[5-8,13] In addition, they also have fueled a debate regarding the extent to which secondary gas-phase reactions accelerate the decomposition of TMIn.

These discrepant experimental observations are further burdened by the results of recent theoretical work. Quantum-level calculations predicting thermochemical properties, such as BDEs and heats of formation (ΔH_f), have recently been published for TMIn and support a much stronger $(CH_3)_2In\text{-}CH_3$ bond energy for this compound. The most accurate *ab initio* molecular orbital and density functional calculations published to date for indium compounds indicate that the BDE for the $(CH_3)_2In\text{-}CH_3$ bond is 10-15 kcal mol^{-1} stronger than the largest value (54 kcal $mole^{-1}$) ever extracted from flow-tube investigations.[14] Although the accuracy of these calculations for indium-containing compounds is difficult to establish due to a lack of reliable experimental data, the *ab initio* methods produce results which are in good agreement with values accepted for the simple chlorides $InCl_3$ and InCl. In addition, agreement between calculated and experimental energetics for Group IIIA compounds higher in the periodic table is good. Thus, the validity of the experimental methods must be called into question.

Taking into account the degree of variability in the experimental observations, and the large differences between measured and predicted bond strengths, it is our belief that the analyses of all hot-wall flow-tube data reported thus far for TMIn are flawed. The deleterious influences of carrier-gas effects and heterogeneous reactions result in an unreliable measurement of the activation energy for reaction [1]. Therefore, in an effort to better understand the behavior of TMIn in flow-tube reactors, we investigated the pyrolysis of this compound in various

chemical environments using modulated molecular-beam mass spectrometry and detailed numerical modeling. The experimental evidence suggests that TMIn decomposition in this type of reactor is preceded by a short induction period indicative of an autocatalytic process. After activation of the tube walls, the thermolysis exhibits a limiting or steady-state behavior that is *completely* surface mediated. To our knowledge these observations have not been reported for the TMIn system, indicating that current mechanisms for pyrolysis in flow-tube reactors are incorrect, as are the energetics of bond cleavage derived from these experiments.

II. Experimental

Apparatus and Measurements. The experimental apparatus is described in detail elsewhere.[13,15] It consists of a high-temperature flow reactor (HTFR) comprising a water-jacketed steel vacuum chamber that contains alumina- and graphite-felt insulation, resistive heating elements, and a flow tube interfaced to a molecular-beam mass spectrometer. The essential elements of the system are a quartz flow tube 6.4 cm in diameter and 112 cm in length, a water-jacketed translating injector for admission of thermally sensitive reactants, a differentially-pumped vacuum manifold for extraction of gas samples, and a quadrupole mass spectrometer (Extrell C50) with better than unit resolution up to 500 AMU. Mass flow controllers are used to meter all gas feed rates. The reactor exhaust is throttled, allowing for feedback control of the reactor pressure to any desired setpoint within the range 1 to 760 Torr. Power to the heating elements is also under feedback control which provides for a stable centerline temperature that is ± 2 K about the setpoint over 80% of the heated length. Residence times in excess of 2 s can be achieved by adjusting the injector position, total flow rate, pressure, and temperature.

Gases exiting the flow tube are sampled using a molecular-beam expansion through a small orifice that is located within the last 4 cm of the quartz tube. The flow exiting the orifice is supersonic and under-expanded, creating a rotationally cold and collisionless neutral beam that is

subsequently chopped by a resonant modulator driven at 800 Hz and ionized by electron impact at 24 eV. The ion signals from the electron multiplier are collected in either one of two modes: (1) the amplified output is directed through an A/D board and digitized continuously as the experiment proceeds (these data will be referred to as analog ion signals); (2) the chopper reference and electron multiplier signals are routed through a lock-in amplifier where the modulated ion signals are extracted from the DC baseline. This allows for discrimination between beam gases and background gases that are present in the quadrupole chamber thereby increasing the sensitivity of the instrument. These data will be referred to as modulated ion signals. The analog mode is used for fast data-tracking at rates greater than 50 Hz per mass channel, while the modulated mode is used for quantifying gas-phase concentrations of product and reactant species and is limited to data collection rates of 1-5 Hz per mass channel.

The pyrolysis of TMIn was investigated at 573, 673, and 723 K in carrier gas mixtures of He, H_2, D_2, C_2H_4 and a trace amount of Ar at a total pressure of 15 Torr. The chemical injector was held at a fixed position within the reactor, while the total gas flow rate was adjusted to maintain a constant residence time of 0.3 s in the hot zone. TMIn (Epichem) was fed from a manufacturer-supplied bubbler via He carrier gas and diluted to an initial mole fraction of $(8.5\pm0.3)\times10^{-4}$. The temperature and back pressure within the bubbler unit were actively controlled such that the delivery rate of TMIn was stable and constant throughout the investigation. Prior to the introduction of TMIn, the reactor tube was cleaned at 873 K with a gas mixture containing 3% HCl for 15 minutes; this was necessary to remove deposits of indium compounds from previous runs.

Experiments were conducted by introducing TMIn into the reactor through the injector and monitoring ion signals as a function of time at m/e ratios of 150, 145, 115, 40, 30, 17, and 16, which correspond respectively to the ions $InCl^+$, $C_2H_6In^+$ (a marker for TMIn), In^+, Ar^+, $C_2H_6^+$, CH_3D^+, and CH_4^+. All ion signals were normalized to an internal standard of argon in order to minimize the effects of gas composition on recorded signals, which proves to be an

effective method for extracting quantitative information from beam studies.[15,16] Mass flow controllers attached to pure gas sources were used to calibrate the system for C_2H_6 and CH_4. The same calibration factors measured for CH_4 were used to quantify the CH_3D ion signals.

Numerical Method. In addition to the experimental work, a numerical model was used to further investigate the nature of the surface-mediated steady-state behavior of TMIn in our reactor. To simulate the fluid dynamics and chemistry of the flow tube, we used the CRESLAF[17,18] and CHEMKIN[19] software packages. CRESLAF is a FORTRAN program that predicts the velocity, temperature, and species profiles in two-dimensional channels (planar or axisymmetric). The model uses a boundary-layer approximation to solve the coupled hydrodynamic and species continuity equations. As such, there must exist a principal flow direction in which convection dominates diffusive transport, a criteria that is always met under the laminar-flow conditions of these experiments. The model accounts for finite-rate gas-phase and surface chemistries, as well as multi-component molecular transport, via the CHEMKIN, SURFACE CHEMKIN, and transport interpreters,[20] respectively. These three software packages compose a body of subroutines that are linked to CRESLAF, creating a standard platform from which to calculate equations of state, chemical production rates, thermodynamic properties, and mass diffusivities. For a complete discussion on CRESLAF and the CHEMKIN packages, the reader is referred to the above literature citations and the references therein.

The model predictions of species concentration profiles within the reactor were used to calculate the mole fractions of hydrocarbons produced during thermolysis of TMIn. These predictions were then compared to experimental values measured under various reactor conditions in order to support or refute proposed reaction schemes. Specifically, we wanted to investigate the significance of gas-phase radical reactions during surface-mediated decomposition of TMIn. The pertinent reaction schemes will be developed in a subsequent section.

III. Results of HTFR Experiments

In order to better understand the chemical reactions involved in thermolysis of this important MOCVD precursor, the pyrolytic behavior of TMIn was investigated at 573, 673, and 723 K in five different carrier gas compositions: pure He; a 90:10 mix of $He:C_2H_4$; a 50:50 split of $He:H_2$ or $He:D_2$; and a 40:50:10 mix of $He:H_2:C_2H_4$. Our observations are consistent with previous investigations in regards to:[5-8,12] (1) the hydrocarbon products formed during pyrolysis, primarily CH_4 (or CH_3D) and C_2H_6, (2) the acceleration of TMIn decomposition in H_2 carrier gas, and (3) the presence of surface deposits within the hot zone of the reactor. However, this work differs from previous investigations in that the initial stages of TMIn decomposition were closely monitored in order to explicate the role of heterogeneous chemistry. To this end, the reactor tube was always cleaned prior to TMIn exposure, meaning that pertinent observations were never made in a *seasoned* vessel, as was the case in all previous flow-tube studies.

Illustrated in Figure 1 is an analog scan of the $C_2H_6In^+$ (m/e 145) ion signal as a function of time for TMIn exposures at 573, 673, and 723 K in pure He carrier gas at 15 Torr and at a constant residence time of 0.3 s. At 573 K, the TMIn ion signal reaches a constant value shortly after its introduction into the reactor. This condition serves as a signal baseline and represents an unreactive state. At 673 K the signal behavior is quite different; the ion trace attains the same value as the unreactive state for approximately 5 min then decreases over a period of several minutes and plateaus at times longer than 14 min. The signal level at the plateau indicates that approximately 60% of the TMIn has decomposed. For a reactor temperature of 723 K, the TMIn signal nearly attains the value of the unreactive state, but drops quickly to zero indicating 100% decomposition of the TMIn.

It is clear from the ion signals in Figure 1 that TMIn decomposition in flow-tube reactors is preceded by an induction period during which the walls become activated. The chemical composition of the active surface likely contains indium and perhaps carbonaceous material in

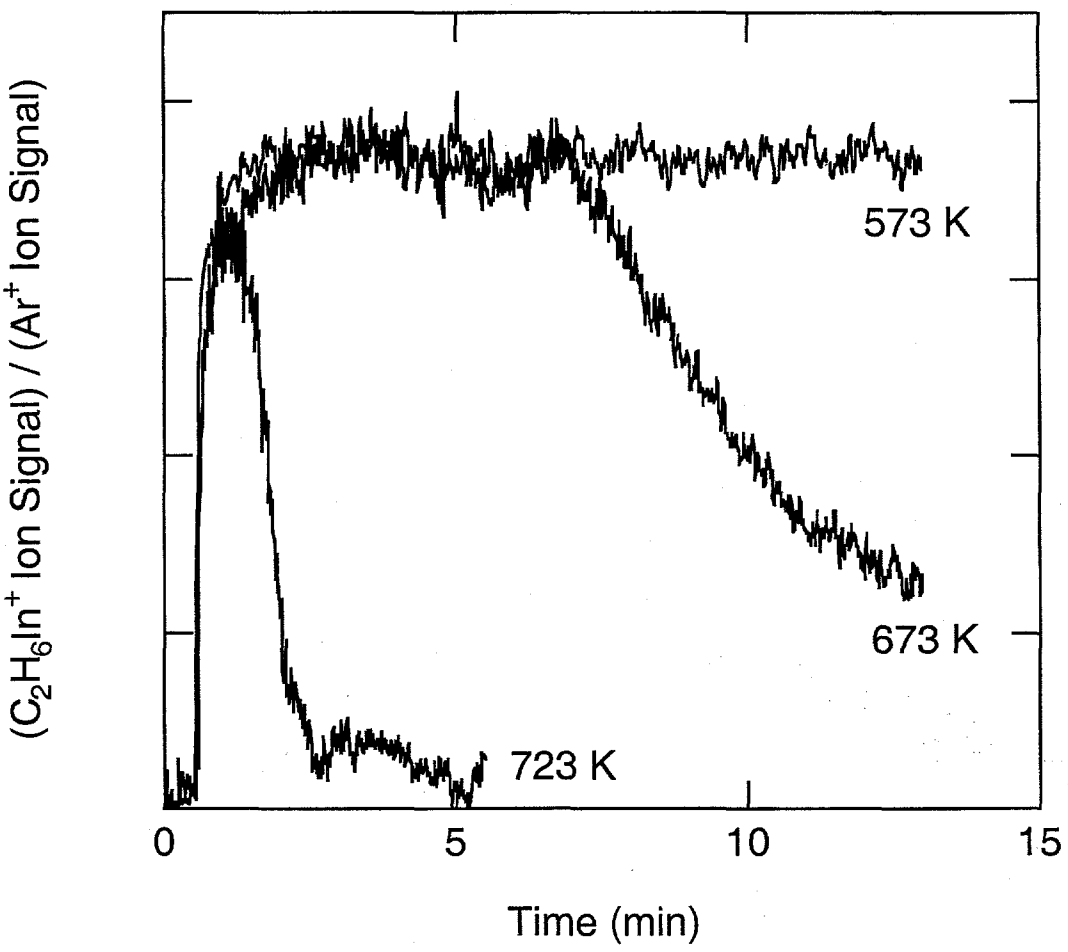

Figure 1. Analog scan of the normalized $C_2H_6In^+$ (m/e 145) ion signal as a function of reaction time at 573, 673, and 723 K for a constant residence time of 0.3 s in He carrier gas at 15 Torr. TMIn is introduced into the reactor at 0.5 min.

the form of CH_x groups, which has been suggested in the past.[6,7] The results of our tube-cleaning procedure substantiate these assumptions. Shown in Figure 2 are the analog scans of the CH_4^+/CH_2D^+ (m/e 16) and $InCl^+$ (m/e 150) ion signals as a function of time during exposure to a gas flow containing 3% HCl in pure He. These data were collected after a typical experiment and serve to identify the nature of the deposits found on the tube wall following TMIn decomposition. Gas flows containing TMIn and D_2 were discontinued for a period of at least 5

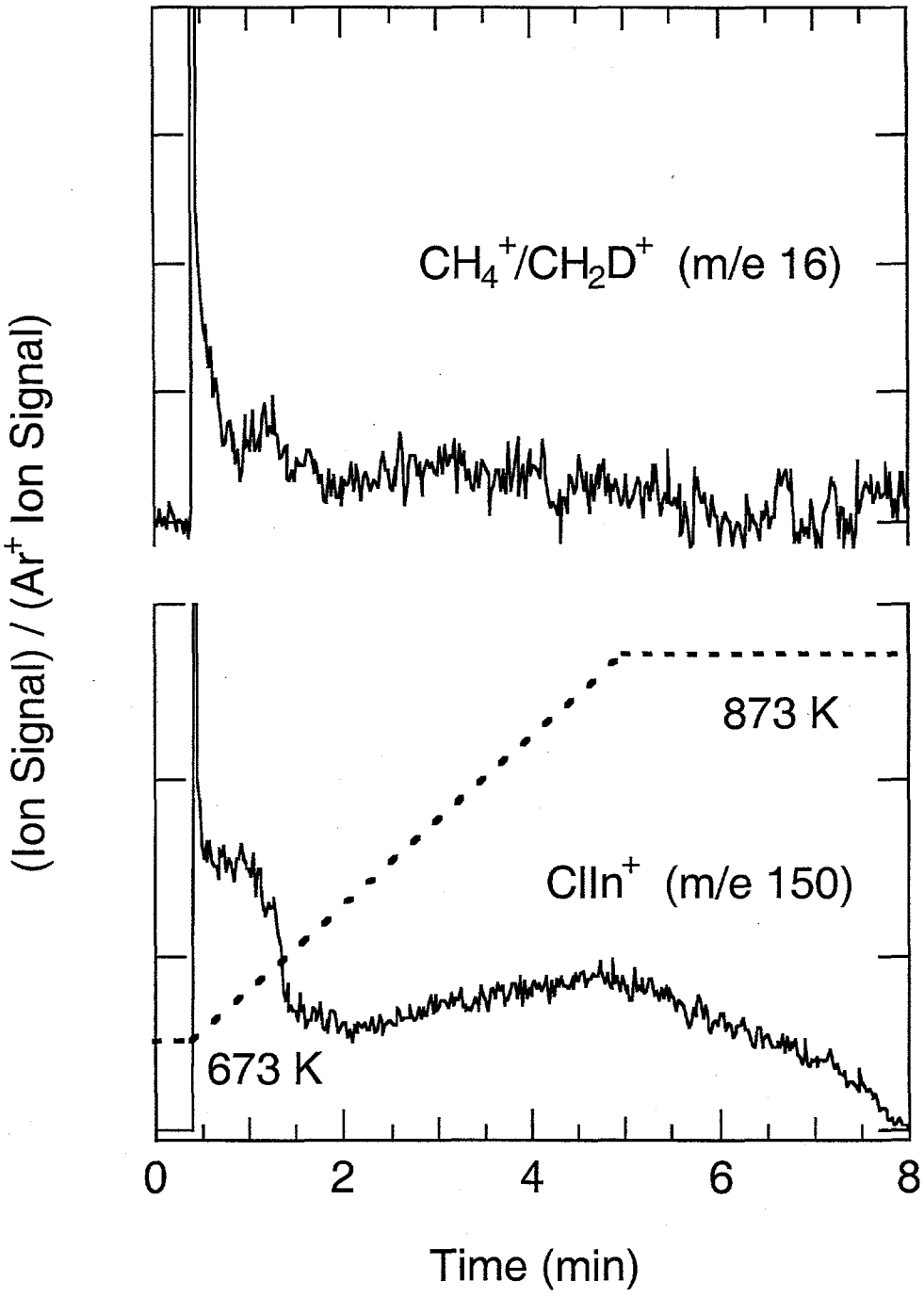

Figure 2. Analog scans of the normalized ion signals for CH_4^+/CH_2D^+ (m/e 16) and $ClIn^+$ (m/e 150) as a function of etch time taken at the conclusion of a 20-minute exposure to TMIn in a 50:50 mix of He:D_2. HCl (3% by volume) is introduced into the reactor at 0.4 min, from 0.4 to 5 min the reactor temperature is ramped from 673 to 873 K (dashed line).

min prior to HCl addition in order to ensure complete purging of these compounds from the reactor vessel.

Consulting Figure 2, HCl was added to the carrier flow at 0.4 min, at which time a ramp in the reactor temperature from 673 to 873 K was initiated. When HCl is first introduced into the reactor, CH_4 and a chloride of indium ($InCl_x$, x=1,2,3) are seen in the exhaust gases. No mass peaks are observed above 150 AMU; however, the m/e 150 mass feature cannot be definitively assigned to the subchloride InCl without further knowledge of the fragmentation pattern of the other chlorides (x=2,3). At times between 0.4 and 1.5 min, a large burst of $InCl_x$ coincident with the CH_4 peak occurs, after which the CH_4 vanishes and the $InCl_x$ signal drops by a factor of 3. The reactor temperature reaches 873 K at approximately 5 min, where the $InCl_x$ features peak and then gradually drop to zero. The data in Figure 2 indicate that stable surface species persist on the tube wall after TMIn exposure at 673 K and may be volatilized by adding HCl and heating the reactor to 873 K.

There appear to be at least two types of adsorbates on the reactor walls that can be identified by reaction with HCl, one containing the CH_xIn (x=1,2,3) group and the other indium. The sharp drop in the $InCl_x$ signal at 1.5 min may suggest a transition from removal of adsorbed CH_xIn groups to the removal of bulk indium, the latter having a greater energy barrier to reaction with HCl than the former. In any event, after the acid etch the quartz reactor is clean and a mixture of white and yellow crystallites (presumably $InCl_X$) can be found in the colder regions of the exhaust manifold downstream of the flow tube.

Carrier-Gas Effects. A principal observation of TMIn thermolysis is that the relative reactivity of the carrier gas changes the apparent rate of decomposition. Shown in Figure 3 are the modulated ion signals for $C_2H_6In^+$ as a function of time during exposure to TMIn at 673 K in various carrier-gas environments. Listed in Table 1 are the induction times and the steady-state conversions of TMIn for each of the reactor conditions investigated. The length of the induction

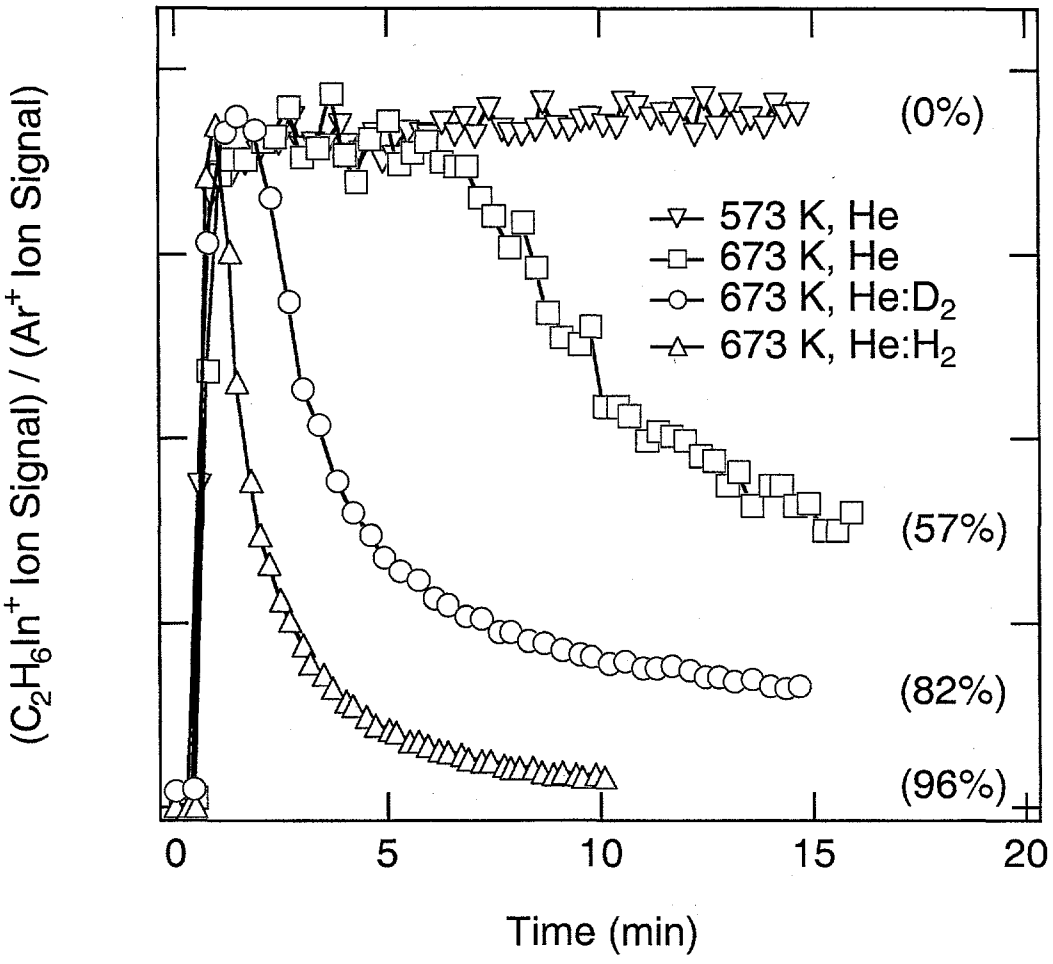

Figure 3. Modulated ion signal for $C_2H_6In^+$ (m/e 145) as a function of reaction time at 573 and 673 K, a constant residence time of 0.3 s, in various carrier gas compositions at 15 Torr. TMIn is introduced into the reactor at 0.5 min. The numbers in parenthesis indicates percent conversion at steady-state.

period was calculated from the time difference between the points at which the TMIn and C_2H_6 signals began to depart from the baseline, the former indicating the beginning of TMIn exposure and the latter indicating that the decomposition rate had increased to a measurable level. Two pertinent observations are apparent in Figure 3 and Table 1. First and foremost, the initial TMIn signal always rises to the level of the unreactive state regardless of the carrier-gas composition, and secondly, switching from pure He to 50:50 mixtures of $He:D_2$ and then $He:H_2$ decreases the

Table 1. Induction time, steady-state conversion, and hydrocarbon product mole fractions for TMIn pyrolysis as a function of carrier gas composition at 673 K, a reactor pressure of 15 Torr, and an initial TMIn mole fraction of $(8.5\pm0.3)\times10^{-4}$.

carrier gas	mixing ratio	ind. time	conversion	CH_4 or CH_3D	C_2H_6
		(min)	(%)	[b](mole fraction $\times10^{-4}$)	
[a]He	---	4.6	57	0.1±0.1	7.8±0.3
He:D_2	50:50	1.3	82	2.5±0.1	8.5±0.2
He:H_2	50:50	0.3	96	7.1±0.3	8.7±0.1
He:C_2H_4	90:10	2.3	62	0.2±0.1	7.1±0.2
He:H_2:C_2H_4	40:50:10	1.2	89	5.3±0.3	7.7±0.3

(a) Decomposition of TMIn in He carrier gas is not at steady-state after 15 minutes of reaction (see text). (b) The reported uncertainty is based upon the precision of the measurement at the 95% confidence interval and as such represents the scatter in the data.

induction time from 4.6, to 1.3, to 0.3 min with a concomitant increase in the steady-state conversion of TMIn from 57, to 82, to 96%, respectively.

The composition of the carrier-gas also affects the distribution of hydrocarbon products formed during TMIn pyrolysis. Figure 4 illustrates the time-dependent behavior of the mole fractions for C_2H_6, CH_4, and CH_3D measured during TMIn exposure at 673 K. Here, C_2H_6 is the only gas-phase product of consequence formed in pure He. Upon the addition of H_2 (D_2), CH_4 (CH_3D) is produced in addition to C_2H_6. The delay in the onset of hydrocarbon production is coincident with the break-point of the TMIn signals in Figure 3, which emphasizes the strong correlation between $C_2H_6In^+$ ion signals (TMIn marker) and the progress of the decomposition reaction. The large spike of short duration in the CH_4 signal for the He and He:H_2 cases in Figure 4 is due to the accumulation of CH_4 in the source bubbler and not to chemical reactions occurring within the flow tube. The absence of a spike in the CH_3D signal (filled circles, m/e 17) supports this notion because this compound is not a byproduct of TMIn decomposition within the bubbler.

Listed in Table 1 are the steady-state values of the hydrocarbon mole fractions taken from the data in Figure 4. It is evident that the limiting or steady-state mole fraction of C_2H_6, which averages $(8.3\pm0.5)\times10^{-4}$ for decomposition in the absence of C_2H_4, is nearly independent of the

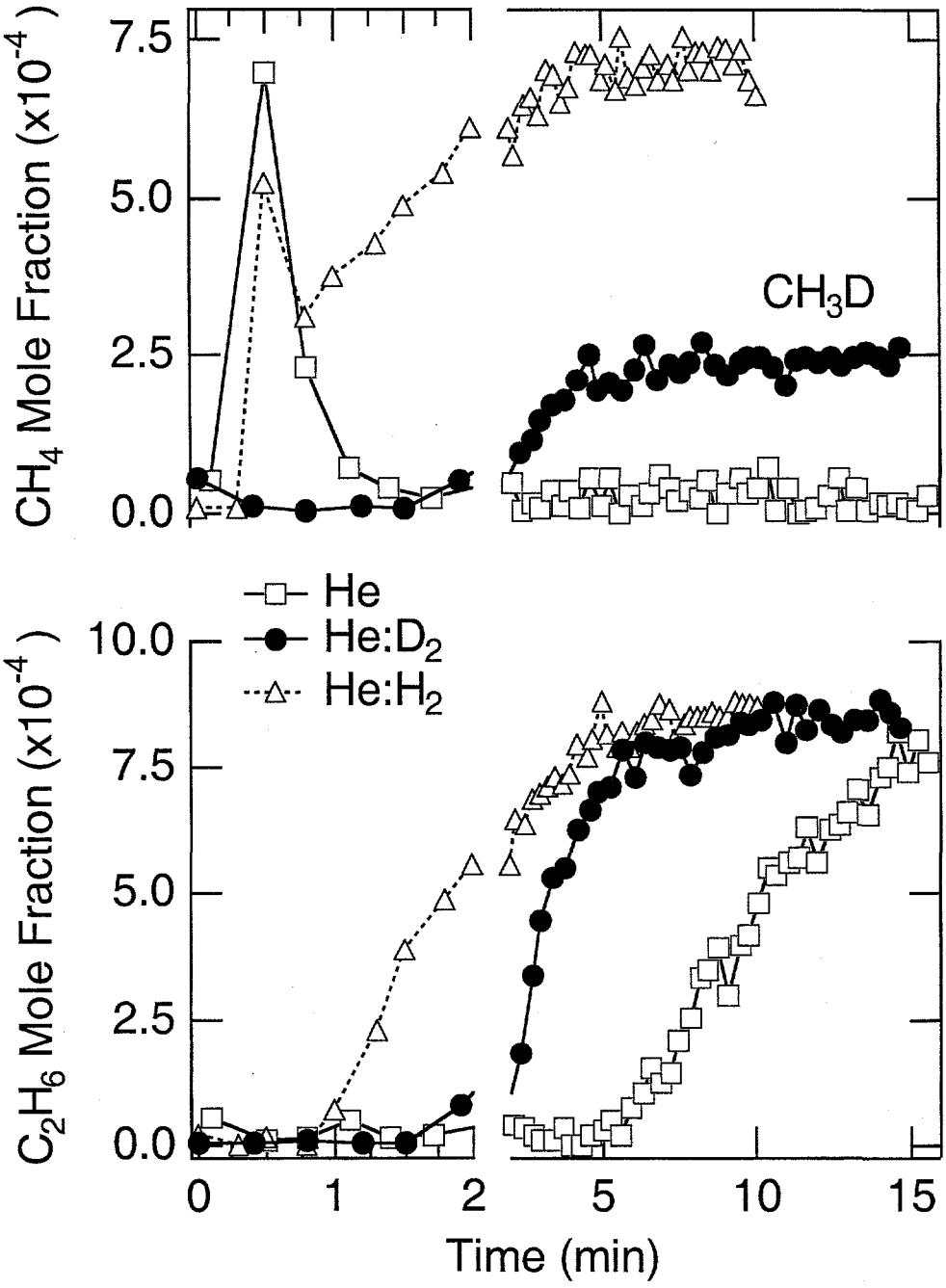

Figure 4. Mole fractions of CH_4 (or CH_3D) and C_2H_6 measured as a function of reaction time at 673 K, a constant residence time of 0.3 s, in various carrier gas compositions at 15 Torr. The abscissa has been expanded below 2 min in order to resolve early transients.

carrier-gas composition. Conversely, the formation of CH_4 or CH_3D is a direct result of adding H_2 or D_2 and is thereby dependent on the carrier-gas composition. In addition, the amount of CH_3D formed during decomposition in $He:D_2$ is a factor of 3 less than the amount of CH_4 produced in $He:H_2$. This correlates well with the lower steady-state conversion of TMIn in $He:D_2$ mixtures and is most likely the result of a kinetic isotope effect.

Ethylene Addition. A natural hypothesis that can be proposed from the observed pyrolysis behavior of TMIn in H_2 (D_2) is that the additional chemistry is driven by reactions of gas-phase CH_3 and H radicals with H_2 (D_2). These processes are well documented within the combustion literature and can certainly account for the formation of CH_4 in H_2,[21] as well as the acceleration of TMIn decomposition, provided that these reactions are initiated and then further propagated in the gas-phase.

To test this hypothesis we added C_2H_4 (10% by volume), which effectively converts H and CH_3 to longer-chain radicals (C_2H_5 and C_3H_7) by insertion into the carbon-carbon double bond,[22,23] to the carrier flow for TMIn pyrolysis in pure He and a mixture of $He:H_2$. Presented in Figure 5 are the modulated ion signals for $C_2H_6In^+$ as a function of time during exposure to TMIn at 673 K in pure He, a 90:10 mixture of $He:C_2H_4$, a 50:50 mixture of $He:H_2$, and a 40:50:10 mixture of $He:H_2:C_2H_4$. It is readily apparent from the ion signals that the presence of C_2H_4 affects the length of the induction period for both the He and $He:H_2$ cases (see Table 1). The induction time decreases by a factor of 2 relative to that in He, and increases by a factor of 4 relative to the time observed for the $He:H_2$ mixture. The data in Table 1 also indicate that C_2H_4 exerts a minor influence (changes of order less than 10%) on the steady-state conversion of TMIn. However, the initial thermal stability of TMIn has not been altered, as evidenced by the maximum in the $C_2H_6In^+$ ion signals for each experiment, which are all approximately the same intensity and equal to that of the unreactive condition (573 K, He ambient).

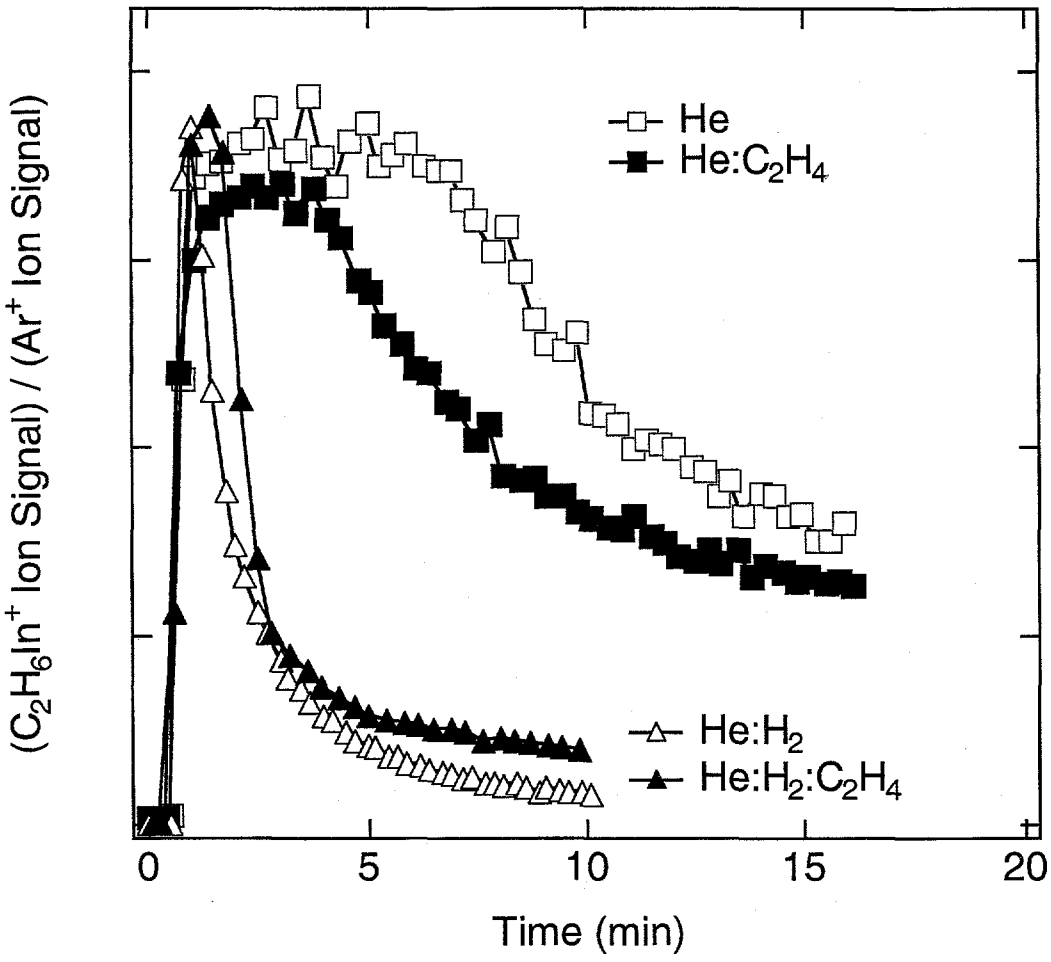

Figure 5. Modulated ion signal for $C_2H_6In^+$ (m/e 145) as a function of reaction time at 673 K, a constant residence time of 0.3 s, in various carrier gas compositions at 15 Torr. TMIn is introduced into the reactor at 0.5 min.

The addition of C_2H_4 also changes the hydrocarbon product distribution, as evidenced by the data presented in Table 1. The steady-state mole fractions for C_2H_6 decrease by roughly 11% for each case, while the production of CH_4 in He verses $He:C_2H_4$ remains unchanged within the experimental uncertainty. The largest effect of C_2H_4 addition can be seen on the amount of CH_4 measured in a $He:H_2$ mix verses the 40:50:10 split of $He:H_2:C_2H_4$, where the amount of CH_4 decreases by 25%. In addition to a decrease in the amount of C_1 and C_2 hydrocarbons produced, we also observed the appearance of mass peaks at m/e of 44 and 43, which correspond to longer-

chain C_3 and C_4 moieties. No attempt was made to quantify the amount of C_3 and C_4 produced in these experiments, but it was noted that the relative intensity of the m/e 44 and 43 signals were greater in the presence of H_2 than in the He:C_2H_4 experiment.

Summary of HTFR Experiments. While earlier investigators have documented the relative increase in the apparent rate of TMIn decomposition in H_2 (D_2) ambients,[6,7,12] as well as the change in hydrocarbon product distribution,[6,7] they did not describe any transient behaviors of TMIn pyrolysis in their flow-tube reactors. Our experimental observations indicate that thermal decomposition of TMIn is a process involving complex heterogeneous reactions. An initial incubation period is followed by an exponential increase in the consumption of TMIn which, after a relatively short period of time, exhibits steady-state behavior.

The initial stages of this reaction are affected by the presence of H_2 or D_2 in the carrier gas; these compounds can increase the reactivity of the flow-tube environment by participating in the propagation of radical chain reactions. The addition of H_2 or D_2 to the carrier-gas mixture decreases the induction time relative to the pure He case, increases the rate of TMIn conversion at steady-state, and creates CH_4 or CH_3D. In addition, the extent of pyrolysis is greatest in mixtures of He:H_2 and decreases in He:D_2, with the least reactive state observed for pure He carrier gas. Adding C_2H_4 to perturb the gas-phase radical pool affects the induction times for both He and He:H_2, creates longer chain alkyls (C_3 and C_4), presumably indicating the presence of gas-phase CH_3 and H, and decreases by 25% the amount of CH_4 produced in He:H_2 mixtures. The composition of the carrier gas does not, however, affect the initial thermal stability of TMIn nor does it strongly influence the steady-state production rate of C_2H_6 at 15 Torr and 673 K.

These new results strongly suggest that existing concepts concerning the thermal stability of TMIn, and accepted mechanisms for its decomposition by gas-phase reactions during MOCVD, are likely to be in error. Consequently, past speculation as to the exact nature of carrier-gas effects, specifically the supposition that gas-phase radical reactions are responsible

for an increase in the apparent rate of TMIn decomposition, may also be in error. These ideas will be explored numerically in the next section of this manuscript.

IV. Results of Numerical Experiments

The intention of the numerical work is not to address issues related to the transient aspects of surface activation, but instead to focus on the steady-state pyrolysis of TMIn in hot-wall flow-tube environments. Our specific objective is to formulate plausible mechanisms for TMIn decomposition, and to evaluate the relative importance of gas-phase radical processes in this system as they pertain to the observed carrier-gas effects and conversion efficiency. To accomplish this task, various reaction mechanisms are developed, incorporated into the flow model, and then tested by comparing simulated hydrocarbon product distributions to experimental data.

Mechanism Development. In order to model the observed steady-state behavior of TMIn in our flow-tube reactor, we combine irreversible global surface reactions with a comprehensive elementary gas-phase mechanism. The use of global surface reactions maintains the premise that TMIn decomposition is initially heterogeneous, while minimizing the difficulty of resolving thermochemistry and elementary kinetics for a complex surface-mediated process. The net effect is to provide a simple route for conversion of TMIn to hydrocarbons and reactive intermediates, which then desorb into the gas. Once the decomposition products have volatilized, they are free to participate in numerous well-defined abstraction, elimination, initiation, and propagation reactions. This method provides an effective means to investigate the significance of gas-phase radical chemistry and to identify key rate-limiting processes.[15]

Listed in Tables 2 and 3 are the reactions incorporated into the flow model. There are three global surface mechanisms, labeled S1 to S3 (Table 2), and two gas-phase mechanisms labeled G1 and BLS (Table 3). Simulations that combine one surface mechanism with either G1

or BLS were used to test the relative importance of gas-phase and surface chemistries to TMIn decomposition.

Table 2. Global surface reaction mechanisms used to simulate the effects of carrier gas composition on steady-state TMIn pyrolysis at 673 K and 15 Torr.

no.	[(a)]global surface reactions	A	β	[(b)]E
S1	$In(CH_3)_3 + In(s) \rightarrow \frac{1}{2}(3\text{-}x)C_2H_6 + xCH_3 + In(s) + In(b)$	2.07×10^{13}	-0.5	46170
S2	$In(CH_3)_3 + In(s) \rightarrow \frac{1}{2}(3\text{-}x)C_2H_6 + xCH_3 + In(s) + In(b)$	2.07×10^{13}	-0.5	44170
S3	$In(CH_3)_3 + In(s) \rightarrow (CH_3)_3In(s) + In(b)$	1.0	0.0	0.0
	$(CH_3)_3In(s) \rightarrow \frac{1}{2}(3\text{-}x)C_2H_6 + xCH_3 + In(s)$	6.20×10^{14}	0.0	46170
	$\frac{1}{2}H_2 + \frac{1}{3}(CH_3)_3In(s) \rightarrow CH_4 + \frac{1}{3}In(s)$	1.00×10^{13}	-0.5	57000

(a) Surface-phase rate constant of the form $\gamma = AT^{\beta}\exp[-E/RT]$ which is unitless and in the range $(0 \leq \gamma \leq 1)$, s = surface and b = bulk species. (b) Units of cal mol^{-1}.

The mechanisms S1, S2, and S3 in Table 2 capture the essence of the experimental observations in that TMIn decomposition is entirely heterogeneous. The organometallic molecule impinges onto active indium sites at the surface and, through various elementary reactions that are embodied within one or more global steps, C_2H_6, CH_4, and CH_3 desorb into the gas. The parameter x in these equations is used to adjust the relative amount of C_2H_6 verses CH_3 that enters the gas phase. Mechanisms S1 and S2 are identical except for a 2 kcal mol^{-1} difference in activation energy. This energy difference accounts for an increase in the surface reactivity induced by hydrogen exposure, which is observed experimentally as a carrier-gas effect, and is possibly due to the formation of surface defects as has been suggested by Bartram and Creighton for MOCVD of GaN.[24] However, reducing the activation energy by 2 kcal mol^{-1} does not

Table 3. Elementary gas-phase reaction mechanisms used to simulate the effects of carrier gas composition on steady-state TMIn pyrolysis at 673 K and 15 Torr.

no.	[a]elementary gas-phase reactions	A	β	[b]E
[c]G1	H: 11, 11a			
	C_1: 21-23, 37-39, 101-103			
	C_2: 64, 75, 76, 79-81, 83, 85, 88, 90, 122, 123, 126-128, 133, 137, 138, 141, 148-151, 153, 155, 167			
	C_2H_4 (+M) ⇆ C_2H_2 + H_2 (+M)	1.80×10^{13}	0.0	76000
	low pressure limit:	1.50×10^{15}	0.0	55443
	C_2H_3 + H (+M) ⇆ C_2H_4 (+M)	6.10×10^{12}	0.3	280
	low pressure limit:	9.80×10^{29}	-3.86	3320
	Troe parameters: α = 0.782, T*** = 208, T* = 2663, T** = 6095			
	C_2H_3 + C_2H_3 ⇆ $CH_2CHCHCH_2$	7.13×10^{13}	0.0	0.0
	C_3: 218, 227-237, 240-242, 245, 257-260, 264-266, 288, 292, 299, 300			
	$HCCHCH_3$ + H ⇆ C_3H_6	1.00×10^{14}	0.0	0.0
	CH_2CCH_3 + H ⇆ C_3H_6	5.00×10^{13}	0.0	0.0
	C_4: 342-345, 348, 349, 360-362, 364-368, 372, 374-376, 382, 384, 385, 387			
	$CH_3CHCH_2CH_3$ (+M) ⇆ C_3H_6 + CH_3 (+M)	2.14×10^{12}	0.7	30856
	low pressure limit:	6.32×10^{58}	-12.85	35567
	enhanced third-body efficiencies: H_2 = 2.0			
	n-C_4H_9 (+M) ⇆ C_2H_5 + C_2H_4 (+M)	1.06×10^{13}	0.0	27828
	low pressure limit:	1.90×10^{55}	-11.91	32263
	enhanced third-body efficiencies: H_2 = 2.0			
	n-C_4H_{10} + H ⇆ *n*-C_4H_9 + H_2	2.84×10^{5}	2.5	6050
	n-C_4H_{10} + H ⇆ $CH_3CHCH_2CH_3$ + H_2	5.68×10^{5}	2.4	3765
	n-C_4H_{10} + CH_3 ⇆ *n*-C_4H_9 + CH_4	5.00×10^{11}	0.0	13600
	n-C_4H_{10} + CH_3 ⇆ $CH_3CHCH_2CH_3$ + CH_4	4.30×10^{11}	0.0	10500
BLS	G1			
	H + $In(CH_3)_3$ → $HIn(CH_3)_3$	1.00×10^{13}	0.0	0.0
	CH_3 + $HIn(CH_3)_3$ → CH_4 + $In(CH_3)_3$	1.00×10^{13}	0.0	0.0
	H + $HIn(CH_3)_3$ → H_2 + $In(CH_3)_3$	1.00×10^{13}	0.0	0.0
	$HIn(CH_3)_3$ → CH_4 + $2CH_3$ + In	2.00×10^{9}	0.0	20000

(a) Gas-phase rate constant of the form $k = AT^{\beta}\exp[-E/RT]$ in units of (cm^3 mol^{-1} s^{-1} or s^{-1}). (b) Units of cal mol^{-1}. (c) Numbers refer to reactions listed in Table 2 of Marinov et al.[21], C_a (a = 1-4) refers to the number of carbon atoms in the primary reactant, additional reactions listed here are modifications to the original Marinov mechanism[38, 39].

directly influence the hydrocarbon product distribution nor does it depend on the absolute amount of hydrogen in the system.

In S3, the process of TMIn decomposition occurs in two steps via an alkyl intermediate formed by TMIn adsorption. Here, the surface-bound organometallic either decomposes by desorption of alkyls or reacts with H_2 to produce CH_4. This step provides a direct pathway for accelerating TMIn decomposition in the presence of H_2, via the liberation of an active surface site, that does not rely upon gas-phase intermediates. Here again, the liberation of CH_4 is a concerted process that most likely involves the dissociation of H_2 on the surface to form adsorbed H atoms, which then recombine with alkyl fragments to form CH_4. We chose to avoid such a detailed description in order to simplify the surface reaction scheme, thereby reducing the number of unknown kinetic constants. The sequences S1 through S3 allow for the consideration that all carrier-gas effects in this system are completely surface mediated.

While the desorption of C_2H_6 and CH_4 from alkylated metal[25-28] and semiconducting[29,30] surfaces is not without precedent, the desorption of CH_3 under our experimental conditions should be considered further. A large body of supporting literature exists that documents the desorption of CH_3 radical from semiconductor surfaces after exposure to TMGa and TMIn under ultra-high vacuum conditions.[31-35] In fact, temperature-programmed desorption (TPD) investigations have established methyl loss as a primary route to organometallic decomposition above 650 K. However, the viability of this pathway under MOCVD conditions, which operate at pressures typically in the range of 1 to 760 Torr where surfaces experience high reactant fluxes, has not been established.

Nonetheless, Butler et al.[36] were able to detect appreciable quantities of CH_3 radical in the boundary layer above heated substrates exposed to TMIn using infrared-diode laser spectroscopy in a cold-wall MOCVD apparatus at 7.6 Torr and substrate temperatures below 673 K. Recently, Russell et al.[37] detected the presence of gas-phase CH_3 radicals in a hot-wall pyrolysis chamber using matrix isolation electron spin-resonance (ESR) spectroscopy during the

thermolysis of similar Group IIIA precursors. Therefore, the desorption of CH_3 under MOCVD conditions seems reasonable.

To describe the gas-phase reactions between unstable intermediates and the stable hydrocarbons and/or carrier gases present in the boundary above the surface, we adopted relevant portions of a hydrocarbon combustion mechanism proposed by Marinov et. al. (labeled G1 in Table 3).[21] The subset used here, which borrows from the comprehensive reaction set proposed by Marinov to describe the formation of aromatic and polycyclic aromatic hydrocarbons in fuel-rich methane and ethane flames, contains detailed kinetics and thermodynamics for 97 reversible elementary reactions between He, H, H_2, and 24 hydrocarbon compounds ranging from C_1 to C_4. It also includes pressure and third-body dependencies for the lighter-molecular-weight species. The numbers in Table 3 under the C_a subheadings refer to the reactions listed in Table 2 of Marinov et. al.[21] Additional reactions presented in Table 3 are recent enhancements[38] or modifications[39] to the original work and thereby indicate where G1 deviates from the published version of the Marinov mechanism. In the interest of limiting this discussion to TMIn, the reader is referred to Marinov for more information regarding this extensive hydrocarbon combustion mechanism.

The final reaction sequence (labeled BLS in Table 3) is a combination of G1 and a series of gas-phase reactions between H, CH_3, and $HIn(CH_3)_3$ that were proposed by Buchan et. al.[7] These authors invoked the existence of a gas-phase hypervalent indium compound ($HIn(CH_3)_3$) in order to explain their experimental observations. The BLS reactions do not form a sound kinetic model because, in all likelihood, H abstraction by H or CH_3 from TMIn would result in the production of H_2 or CH_4 along with a methylene-like species of the form $CH_2In(CH_3)_2$, rather than a hypervalent compound. In addition, the unimolecular decomposition of $HIn(CH_3)_3$ is not microscopically reversible. However, the mechanism proposed by Buchan can be considered general in the sense that all gas-phase processes in this system that result in the decomposition of TMIn must involve H and CH_3. Regardless of the byproducts, BLS can be used to test the

validity of a generic gas-phase radical process under the influence of various carrier gas mixtures.

The model chemistry listed in Tables 2 and 3 provides a functional platform from which to evaluate the relative effects of carrier-gas composition on TMIn pyrolysis chemistry in flow-tube reactors. The kinetic parameters (A, β, and E) used to calculate sticking coefficients for the reactions listed in S1, S2, and S3 were fit to TMIn conversion rates that were measured during the current investigation, as well as from previous flow-tube work conducted in our laboratory.[13] The stoichiometric variable x in these equations determines the relative amount of incident carbon that desorbs as CH_3 per unit of TMIn converted. For each set of simulations, x was varied from a minimum of 0, corresponding to no CH_3 desorption, to a maximum of 3, which forces all incident carbon to desorb as CH_3. Comparing model predictions of hydrocarbon product distributions for different values of x to experimental observations is a valuable tool for distinguishing between dominant chemical pathways. The Arrhenius parameters for the reactions listed in G1 and BLS were taken directly from their respective literature sources without modification.

Illustrated in Figures 6 and 7 are the mole fractions of CH_4 and C_2H_6 predicted by CRESLAF as a function of the incident carbon fraction that desorbs as CH_3. This fraction (y) is simply related to x by the expression: $y = x/3$. As indicated in the legends of each graph, the open symbols denote model results for different combinations of surface and gas-phase reaction mechanisms. The cross-hatched bars in each figure are the measured mole fractions bounded by the respective experimental uncertainties. Data presented in the uppermost graphs reflect the product distributions for TMIn decomposition in pure He carrier gas. The middle and lower graphs in Figures 6 and 7 illustrate the effects induced by adding H_2 and C_2H_4 to the simulated chemistry, respectively.

Carrier-Gas Effects. In general, the predictions of each of the proposed mechanisms are consistent with experimental observations in that CH_4 is a byproduct of adding H_2 to the carrier

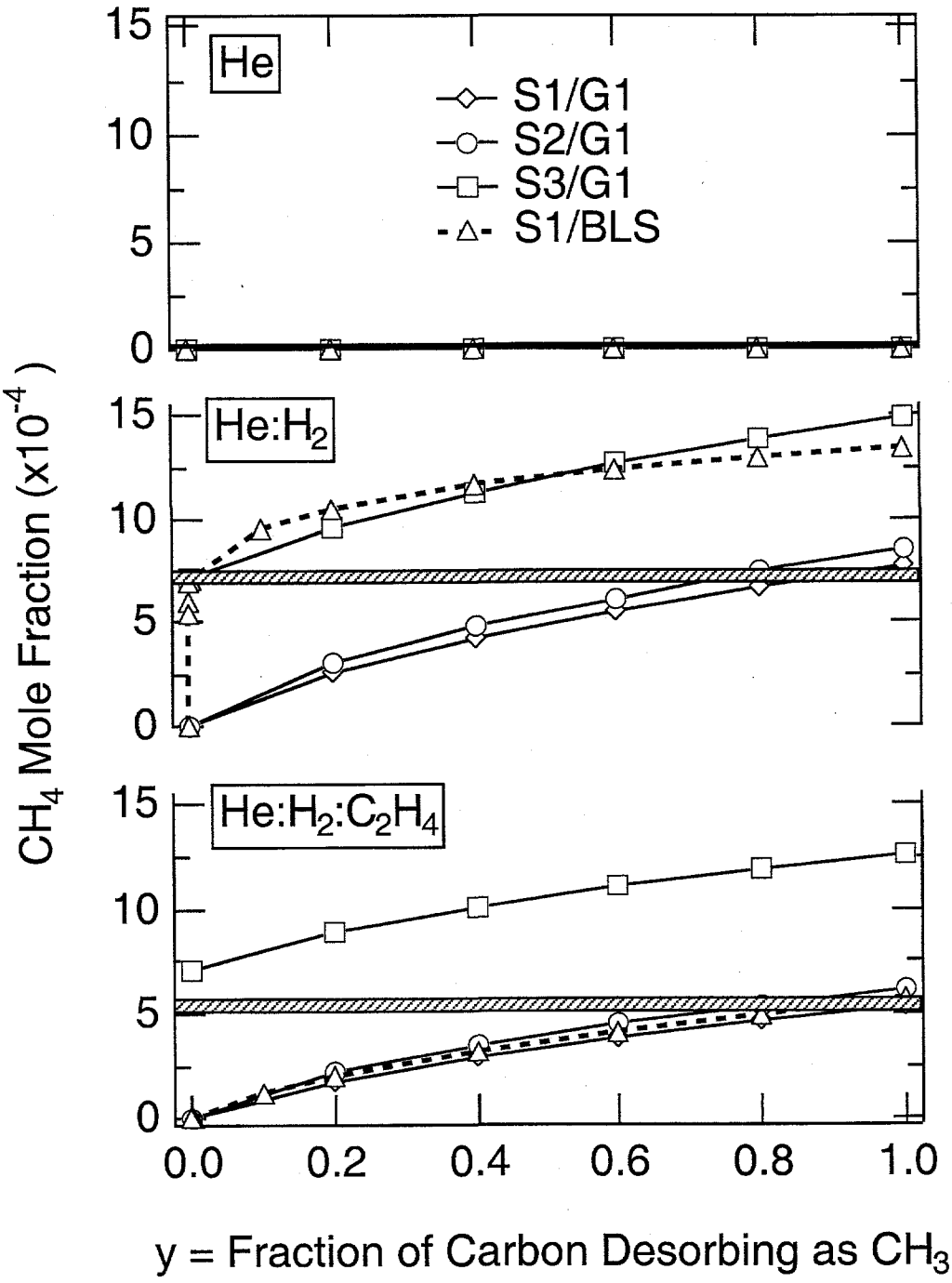

Figure 6. Mole fraction of CH_4 predicted by CRESLAF as a function of the incident carbon that desorbs from the surface as CH_3 radical. The shaded bars indicate upper and lower error bounds of the measured value. [S1/G1], [S2/G1], [S3/G1], and [S1/BLS] are model predictions for different combinations of gas-phase and surface reaction mechanisms (see text).

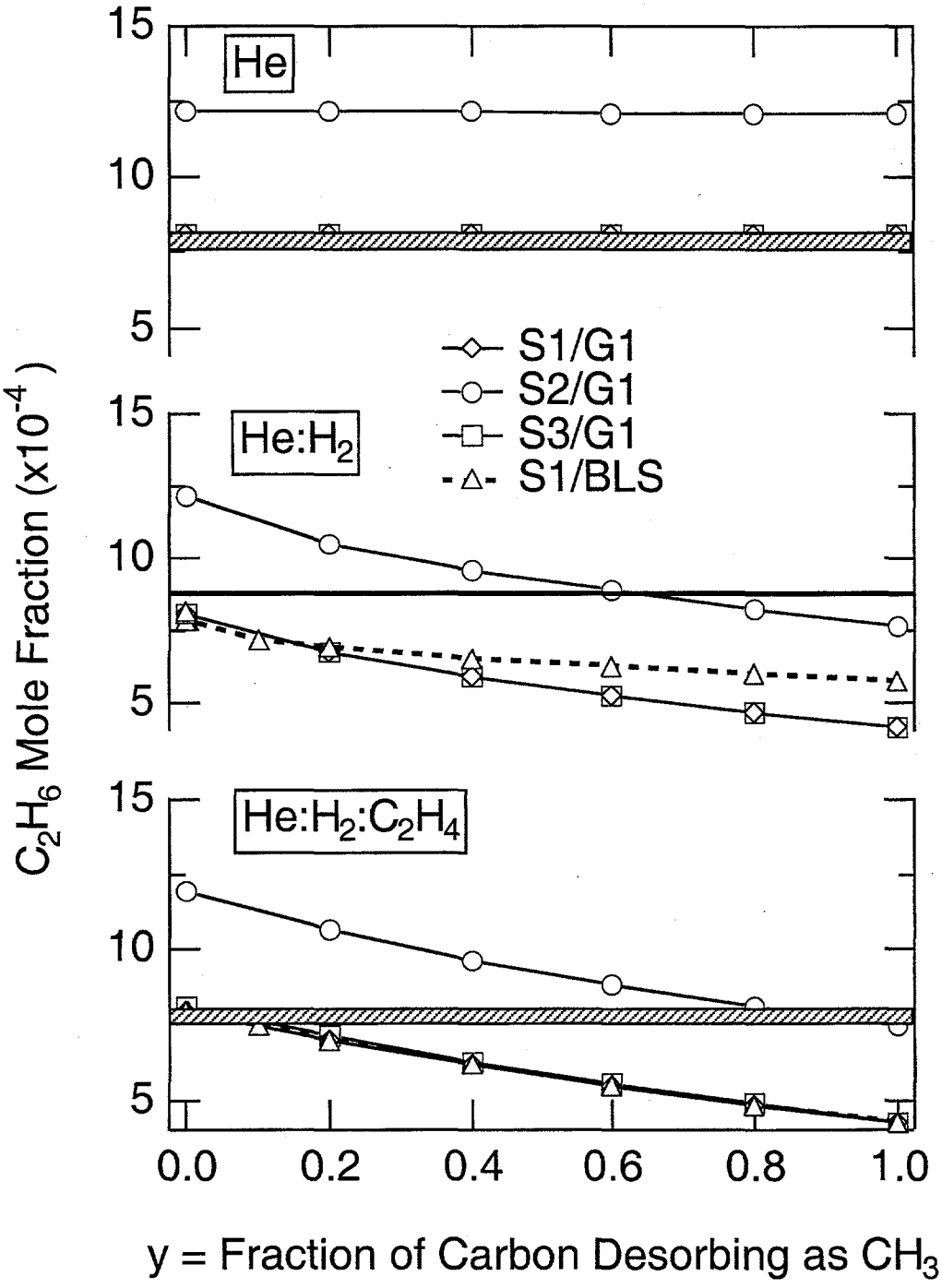

Figure 7. Mole fraction of C_2H_6 predicted by CRESLAF as a function of the incident carbon that desorbs from the surface as CH_3 radical. The shaded bars indicate upper and lower error bounds of the measured value. [S1/G1], [S2/G1], [S3/G1], and [S1/BLS] are model predictions for different combinations of gas-phase and surface reaction mechanisms (see text).

gas. This behavior is evidenced by the uppermost graph of Figure 6, in which all four mechanisms predict no CH_4 formation in pure He. Also, the relative amounts of CH_4 and C_2H_6 formed in either H_2 or H_2:C_2H_4 ambients are dependent upon the fraction of incident carbon desorbed as CH_3, with more CH_4 and consequently less C_2H_6 produced at larger values of y. In addition, a trend in the simulation results has emerged for the fraction desorbed as CH_3; the model predictions are most accurate at either large ($y = x/3 \geq 0.8$) or small ($y = x/3 \leq 0.05$) fractions, but not intermediate.

Focusing on the transition from He to a 50:50 mixture of He:H_2 (upper two graphs in Figures 6 and 7), it appears that mechanisms S3/G1 and S1/BLS are more consistent with experimental observation than either S1/G1 or S2/G1. Reaction set S1/G1 is valid in He carrier gas but fails to predict adequate amounts of C_2H_6 at large y, or CH_4 at small y, in the presence of H_2. This is primarily due to a lower steady-state conversion of TMIn that is carrier-gas independent in this mechanism. In essence, there are no alternate routes for organometallic decomposition in S1/G1 that become active under H_2. Conversely, S2/G1 is valid for He:H_2 mixtures (at $y = 0.80$), yet over predicts the amount of C_2H_6 formed in pure He because conversion of TMIn is too high. The only difference between these two scenarios is a 2 kcal mol^{-1} change in the activation energy for the global surface reaction. If it were possible for H_2 to increase the reactivity of the surface by lowering the energy barrier 2 kcal mol^{-1} without affecting other aspects of the chemistry, then these two mechanisms (S1/G1 and S2/G1) combined would be valid. Additionally, S1/G1 and S2/G1 predict that a substantial portion of the incident carbon ($y = 0.80$) desorbs into the gas as CH_3 during decomposition.

Reaction sets S3/G1 and S1/BLS most accurately reflect the change in hydrocarbon product distributions as the carrier gas composition moves from He to a mixture of He:H_2. Both mechanisms also predict that very little CH_3 ($y \leq 0.05$) needs to desorb from the surface in order to explain the product mixing ratio. What is most interesting about these two scenarios is that S3/G1 does not rely heavily on gas-phase radical reactions for either CH_4 or C_2H_6 formation at

small values of y, whereas the CH_4 production from S1/BLS is entirely homogenous. As a result of these differences, the validity of either mechanism may be distinguished by changing the chemical content of the gas-phase radical pool (e.g., by adding C_2H_4).

Ethylene Addition. The effects of C_2H_4 addition on the hydrocarbon product distributions are illustrated in the lower plots of Figures 6 and 7. Experimentally, the changes observed are relatively minor, with CH_4 production dropping by 25%, C_2H_6 production by 11%, and TMIn conversion by 7% from carrier-gas mixtures of $He:H_2$ to $He:H_2:C_2H_4$ (see Table 1 and Figure 5). C_2H_4 effectively competes with H_2 for H and CH_3, thereby creating longer chain alkyls such as C_3H_6, C_3H_8, and C_4H_{10}, which make CH_4 and C_2H_6 formation slightly less favorable. Therefore, we can surmise at the outset that mechanisms involving substantial gas-phase reactions involving H and CH_3 would be more influenced by C_2H_4 than ones that do not.

All of the S_a/G1 (a = 1,2,3) mechanisms behave as expected in the presence of C_2H_4. We observe that S1/G1 and S2/G1 are more sensitive to a change in carrier-gas composition than S3/G1 because the former reaction schemes necessitate 80% of the incident carbon desorb as CH_3, as opposed to the latter which dictates a much smaller percentage. Under the influence of C_2H_4, S2/G1 is better overall at predicting the decrease in CH_4 and C_2H_6 than either S1/G1 or S3/G1. In fact, the model predictions for S3/G1 in $He:H_2:C_2H_4$ are essentially identical to those in $He:H_2$ because so little of the incident carbon leaves the surface as a reactive intermediate.

The same is not true for the S1/BLS reaction scheme. Even though y is less than 0.05, the data in Figure 6 show a substantial decrease in the CH_4 mole fractions from $He:H_2$ to $He:H_2:C_2H_4$ carrier-gas mixtures. This drop in CH_4 production is accompanied by a 30% decrease in the predicted steady-state conversion of TMIn. In the S1/BLS model, C_2H_4 completely negates the enhanced decomposition of TMIn induced by H_2 addition and therefore is not substantiated by experimental observation, which indicates only a 7% change in the steady-state TMIn conversion (see Table 1 and Figure 5). In this case, the simulations predict that C_2H_4 reduces the gas-phase H-atom concentration by four orders of magnitude and thereby eliminates the interaction

between H and TMIn. In turn, this prevents the formation of hypervalent trimethylindium hydride and the subsequent process of TMIn decomposition and CH_4 production. Of all the mechanisms tested, S1/BLS is clearly the most sensitive to the addition of ethylene and least supported by experimental observation.

Summary of Numerical Experiments. Four separate reaction mechanisms (presented in Tables 2 and 3) were assembled and tested in order to identify major pathways that govern the heterogeneous decomposition of TMIn in hot-wall flow-tube reactors. The mechanisms were incorporated into a two-dimensional boundary-layer code used to simulate the effects of carrier-gas composition on the steady-state hydrocarbon product distribution, and the conversion efficiency of TMIn.

The simulations of C_2H_4 addition conclusively demonstrate that gas-phase reactions proposed by Buchan et al. cannot account for the acceleration of TMIn decomposition in H_2 carrier gas. Moreover, it is unlikely that gas-phase reactions of *any* kind play a substantial role in the thermal decomposition of TMIn at temperatures below 673 K. We believe there is a small presence of CH_3 in the boundary layer above the active surface; however, the chemistry that ensues from this reactive intermediate accounts for less than 10% of the hydrocarbon products and does not influence the rate of TMIn decomposition under the conditions of our experiments. Completely surface-mediated processes, such as those incorporated into mechanism S3, that result in the adsorption of TMIn and H_2, followed by desorption of CH_4 and C_2H_6, appear to be the most important pathways for thermal decomposition of TMIn in hot-wall flow-tube reactors.

V. Discussion and Conclusions

The experiments reported here demonstrate that TMIn pyrolysis in hot-wall flow-tube reactors can be classified as an autocatalytic process. The presence of an induction or incubation period that is thermally activated, followed by an exponential increase in the consumption rate of the organometallic, is behavior consistent with similarly classified metal-deposition reactions of

iron,[40] platinum,[41] and tungsten.[42] After activation of the reactor walls, TMIn decomposition achieves a self-limited, time-invariant conversion rate that can be fit to a first-order kinetic expression. This fact is evident in Figure 8, which is an Arrhenius plot of the rate constant for pyrolysis measured by all previous investigators, including recent work from this laboratory,[13] at a variety of pressures and carrier-gas compositions. All of the aforementioned investigations used hot-wall flow-tube reactors and collected data under steady-state conditions in *seasoned* vessels. The result is a mutually consistent body of work, with a first-order rate constant that varies over 2.6 orders of magnitude, but yields an average activation energy for reaction [1] of 44±6 kcal $mole^{-1}$.

Unfortunately, it is not uncommon for entirely heterogeneous systems to behave in a first-order manner, yielding observations identical to those expected for a unimolecular decomposition. In this instance, it can be very difficult to distinguish between homogeneous and heterogeneous chemistries, due to a complex coupling between the two phenomena.[43-45] In fact, the inability to resolve individual contributions of gas and surface reactions on the observed behavior can invalidate the experimental approach altogether. This seems to be the case for TMIn pyrolysis in hot-wall flow-tube reactors, where the contributions of heterogeneous processes have been overlooked, leading to an underestimation of the bond strengths in TMIn and the belief that this reaction is entirely homogeneous.

The carrier-gas effects observed in this system are not uncommon to thin-film MOCVD processes. There are numerous instances in the literature that describe an increase in the deposition rates for Al,[46] Cu,[47] GaN,[24,48] and CdTe,[49] upon substitution of H_2 for inert carrier gases. In addition to increased film growth rates, these papers have noted a dramatic change in the physical properties of the resulting solid, such as improved morphology and smaller grain sizes, better conformal coverages, and lower film resistivities. It is unclear the extent to which gas-phase reactions are responsible for the observations in these systems. For TMIn however,

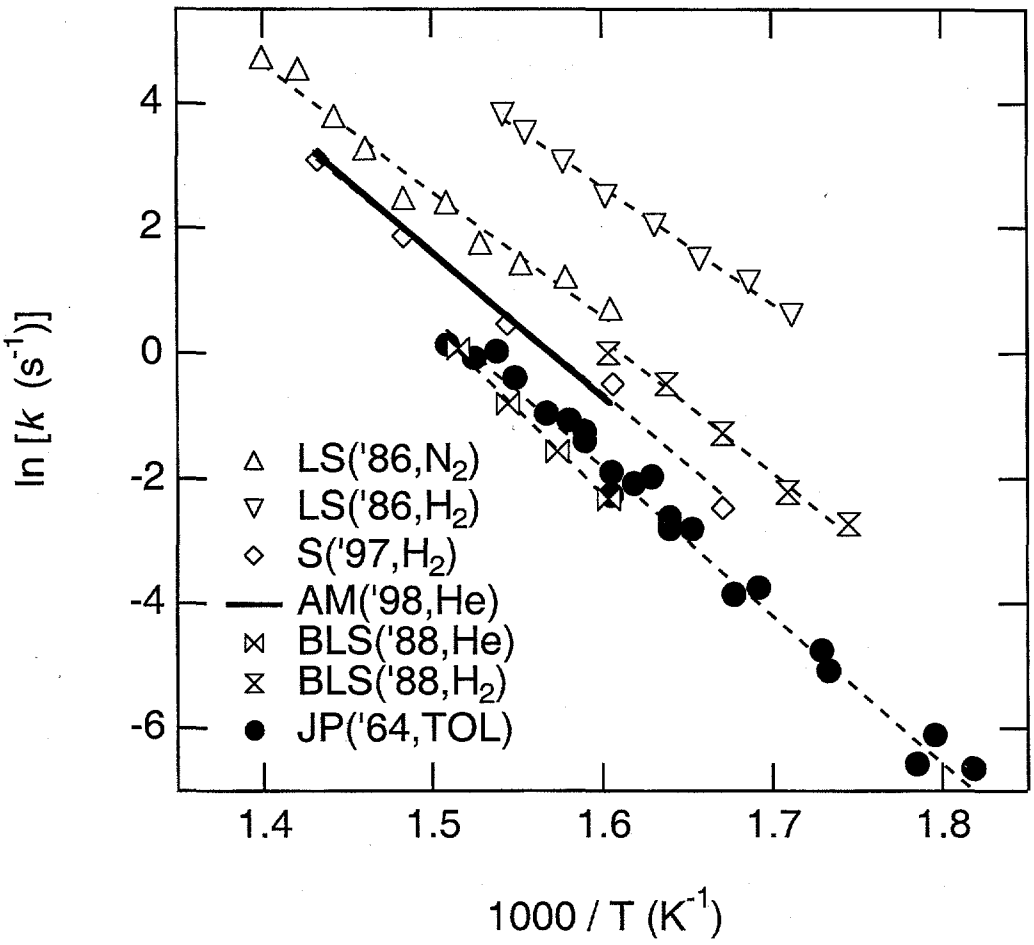

Figure 8. Arrhenius plot for the pyrolysis of TMIn comparing previously published results taken under steady-state conditions in flow-tube reactors. LS=Laresen and Stringfellow[6], S=Sigiyama et. al.[8], AM=Allendorf and McDaniel[13], BLS=Buchan, Larsen, and Stringfellow[7], and JP=Jacko and Price[5].

our numerical work suggests a strong heterogeneity associated with the H_2 chemistry. The simulation results essentially eliminate the likelihood that, at temperatures below 673 K, gas-phase processes either contribute to the thermal decomposition of TMIn or are responsible for a significant fraction of the CH_4 formed under H_2.

The most significant result of this work is the realization that hot-wall flow-tube reactors are inappropriate for investigating pyrolysis of TMIn. It may be possible to generalize this

conclusion to include gallium and possibly aluminum organometallic compounds as well. In looking at TMGa, which is another important group IIIA compound that has been investigated with flow reactors,[50-52] there are striking similarities to the TMIn system. In particular, investigators have observed carrier-gas effects and have reported different energetics and decomposition rates that are dependent upon the surfaces within the reactor. In addition, recent published results of high-level theoretical calculations now suggest that the experimentally determined bond energies for TMGa are too low by 10-15 kcal mol^{-1}.[14,53,54] The kinetic data extracted from the early flow reactor experiments of Jacko and Price and others for TMIn and TMGa have been used extensively by subsequent investigators in formulating mechanistic arguments for MOCVD of IIIA-VA materials.[2,54] The results of this investigation would suggest that conclusions based upon these earlier works should be reexamined.

Acknowledgments. The authors are grateful for the support of this research provided by Libbey-Owens-Ford Co. (Toledo, OH) and the U.S. Department of Energy, Office of Industrial Technologies, Advanced Industrial Materials Program.

References

(1) Davis, R. F. *Proc. IEEE* **1991**, *79*, 702.

(2) Moon, R. L.; Houng, Y.-M. *Organometallic Vapor Phase Epitaxy of III-V Materials*; in *Chemical Vapor Deposition* ; Hitchman, M. L. and Jensen, K. F., Ed.; Academic Press: San Diego, 1993, pp 245.

(3) Ashley, T. *Inst. of Phys. Conf. Series* **1995**, *144*, 345.

(4) Hafizi, M. *Inst. of Phys. Conf. Series* **1996**, *145*, 631.

(5) Jacko, M. G.; Price, S. J. W. *Can. J. Chem.* **1964**, *42*, 1198.

(6) Larsen, C. A.; Stringfellow, G. B. *J. Cryst. Growth* **1986**, *75*, 247.

(7) Buchan, N. I.; Larsen, C. A.; Stringfellow, G. B. *J. Cryst. Growth* **1988**, *92*, 591.

(8) Sugiyama, M.; Kusunoki, K.; Shimogaki, Y.; Sudo, S.; Nakano, Y.; Nagamoto, K.; Sugawara, K.; Tada, K.; Komiyama, H. *App. Surf. Sci.* **1997**, *117*, 746.

(9) Clark, W. D.; Price, S. J. W. *Can. J. Chem.* **1968**, *46*, 1633.

(10) Russell, D. K. *Chem. Vap. Deposition* **1996**, *2*, 223.

(11) Haigh, J.; O'Brien, S. *J. Cryst. Growth* **1984**, *67*, 75.

(12) Haigh, J.; O'Brien, S. *J. Cryst. Growth* **1984**, *68*, 550.

(13) Allendorf, M. D.; McDaniel, A. H. *Mat. Res. Soc. Symp. Proc.* **1998**, *495*, 125.

(14) Allendorf, M. D.; Melius, C. F.; Baushlicher, C. W. J. *J. de Physique IV* **1999**, *9*, PR8-23.

(15) McDaniel, A. H.; Allendorf, M. D. *J. Phys. Chem. A* **1998**, *102*, 7804.

(16) Hsu, W. L.; Tung, D. M. *Rev. Sci. Instrum.* **1992**, *63*, 4138.

(17) Coltrin, M.; Kee, R. J.; Miller, J. A. *J. Electrochem. Soc.* **1986**, *133*, 1206.

(18) Coltrin, M. E.; Moffat, H. K.; Kee, R. J.; Rupley, F. M. *CRESLAF (Version 4.0): A Fortran Program for Modeling Laminar, Chemically Reacting, Boundary-Layer Flow in Cylindrical or Planar Channels*, SAND93-0478 UC-401, Sandia National Laboratories: Albequerque, NM, 1996.

(19) Coltrin, M. E.; Kee, R. J.; Rupley, F. M.; Meeks, E.; Miller, J. A. *Chemkin-III: A Fortran Chemical Kinetics Package for the Analysis of Gas-Phase Chemical and Plasma Kinetics;*

Surface Chemkin-III: A Fortran Package for Analyzing Heterogeneous Chemical Kinetics at a Solid-surface -- Gas-phase Interface., SAND96-8216 UC-405 & SAND96-8217 UC-405, Sandia National Laboratories: Albequerque, NM, 1996.

(20) Kee, R. J.; Dixon-Lewis, G.; Warnatz, J.; Coltrin, M. E.; Miller, J. A. *A Fortran Computer Code Package for the Evaluation of Gas-Phase Multicomponent Transport Properties*, SAND86-8246 UC-32, Sandia National Laboratories: Albequerque, NM, 1986.

(21) Marinov, N. M.; Pitz, W. J.; Westbrook, C. K.; Castaldi, M. J.; Senkin, S. M. *Combust. Sci. and Tech.* **1996**, *116*, 211.

(22) Tsang, W.; Hampson, R. F. **1986**, *15*, 1087.

(23) Holt, P. M.; Kerr, J. A. **1977**, *9*, 185.

(24) Bartram, M. E.; Creighton, J. R., *personal communication*, **1999**.

(25) Lin, J. L.; Bent, B. E. *J. Amer. Chem. Soc.* **1993**, *115*, 6943.

(26) Lin, J. L.; Chiang, C. M.; Jenks, C. J.; Yang, M. X.; Wentzlaff, T. H.; Bent, B. E. *J. Catalysis* **1994**, *147*, 250.

(27) Colin, L.; Cassuto, A.; Ehrhardt, J. J.; Ruizlopez, M. F.; Jamois, D. *Appl. Surf. Sci.* **1996**, *99*, 245.

(28) Chaturvedi, S.; Strongin, D. R. *Langmuir* **1997**, *13*, 3162.

(29) Lin, R.; Masel, R. I. *Surf. Sci.* **1991**, *258*, 225.

(30) Cadwell, L. A.; Masel, R. I. *Surf. Sci.* **1994**, *301*, 415.

(31) Creighton, J. R. *J. Vac. Sci. Technol. A* **1991**, *9*, 2895.

(32) McCaulley, J. A.; Shui, R. J.; Donnelly, V. M. *J. Vac. Sci. Technol. A* **1991**, *9*, 2872.

(33) Zhu, X. Y.; White, J. M.; Creighton, J. R. *J. Vac. Sci. Technol. A* **1992**, *10*, 316.

(34) Aquino, A. A.; Mulcahy, C. P. A.; Jones, T. S. *Surf. Sci. Lett.* **1995**, *344*, L1231.

(35) Wang, H.; Zhu, X. Y.; Xin, Q. S. *J. Vac. Sci. Technol. A* **1998**, *16*, 948.

(36) Butler, J. E.; Bottka, N.; Sillmon, R. S.; Gaskill, D. K. *J. Cryst. Growth* **1986**, *77*, 163.

(37) Russell, D. K.; Mills, G. P.; Raynor, J. B.; Workman, A. D. *Chem. Vap. Deposition* **1998**, *4*, 61.

(38) Marinov, N. M., *personal communication*, **1999**.

(39) Fahr, A.; Laufer, A.; Klein, R.; Braum, W. *J. Phys. Chem.* **1991**, *95*, 3218.

(40) Kellerman, B. K.; Chason, E.; Adams, D. P.; Mayer, T. M.; White, J. M. *Surf. Sci.* **1997**, *375*, 331.

(41) Xue, Z.; Thridandam, H.; Kaesz, H. D.; Hicks, R. F. *Chem. Mater.* **1992**, *4*, 162.

(42) McConica, C. M.; Cooper, K. *J. Electrochem. Soc.* **1988**, *135*, 1003.

(43) Brown, R. L. *J. Res. Natl. Bur. Stand.* **1978**, *83*, 1.

(44) Howard, C. J. *J. Phys. Chem.* **1979**, *83*, 3.

(45) Orkin, V. L.; Khamaganov, V. G.; Larin, I. K. *Int. J. Chem. Kinet.* **1993**, *25*, 67.

(46) Yun, J. H.; Rhee, S. W. *J. Mater. Sci.* **1998**, *9*, 1.

(47) Kim, S.; Park, J. M.; Choi, D. J. *Thin Solid Films* **1998**, *315*, 229.

(48) Schon, O.; Schineller, B.; Heuken, M.; Beccard, R. *J. Cryst. Growth* **1998**, *190*, 335.

(49) McDaniel, A. H.; Wilkerson, K. J.; Hicks, R. F. *J. Phys. Chem.* **1995**, *99*, 3574.

(50) Jacko, M. G.; Price, S. J. W. *Can. J. Chem.* **1963**, *41*, 1560.

(51) Larsen, C. A.; Buchan, N. I.; Stringfellow, G. B. **1988**, *52*, 480.

(52) Hoshino, M. **1990**, *68*, 2538.

(53) Trachtman, M.; Beebe, S.; Bock, C. W. *J. Phys. Chem.* **1995**, *99*, 15028.

(54) Simka, H.; Willis, B. G.; Lengyel, I.; Jensen, K. F. *Prog. Crystal Growth and Charact.* **1997**, *35*, 117.

DISTRIBUTION:

Dr. Charles A. Sorrell
Adv. Industrial Concepts Div., EE-232
U.S. DOE, EE-232
Forrestal Building, 1000 Independence Ave.
Washington, DC 20585

Dr. Charles Bauschicher
NASA Ames Research Center
Mail Stop 230-3
Mountain View CA 94305

Dr. Theodore M. Besmann
Oak Ridge National Laboratories
P.O. Box 2008
Oak Ridge TN 37831-6063

Dr. Donald R. F. Burgess, Jr.
Chemical Science and Technology Lab
NIST
Bldg. 221, Rm B312
Gaithersburg MD 20899

Dr. Christopher E. Dateo
Thermosciences Institute
NASA Ames Research Center
MS 230-3
Moffett Field CA 94035-1000

Dr. Suleyman A. Gokoglu
NASA Lewis Research Center
21000 Brookpark Road
Cleveland OH 44135

Dr. John W. Hastie
National Inst. of Standards & Technology
Ceramics Division
B 106/223
Gaitherburg MD 20899

Dr. Aloysius F. Hepp
NASA Lewis Research Center
21000 Brookpark Road
Cleveland OH 44135

Dr. Nick M. Marinov
Lawrence Livermore National Lab
7000 East Avenue, P.O. Box 808
Livermore CA 94551

Dr. Gerd M. Rosenblatt
Building 50A, room 4119
Lawrence Berkeley Laboratory
1 Cyclotron Road
Berkeley CA 94720

Dr. Wing Tsang
Nat. Institute of Standards & Technology
Gaithersburg MD 20899

Dr. Michael Zachariah
Dept. of Mechanical Engineering
Room 125
Minneapolis MS 55455

Prof. Carmela Amato-Wierda
Dept. of Chemistry
University of New Hampshire
Durham NH 03824

Prof. Timothy J. Anderson
6607 N.W. 44th Place
Gainesville FL 32606

Prof. Peter B. Armentrout
Dept. of Chemistry
University of Utah
Henry Eyring Building
Salt Lake City Utah 84112

Prof. Eray S. Aydil
Chemical Engineering Dept.
University of California
Engineering Building II, Room 3334
Santa Barbara CA 93106

Prof. C Bernard
Laboratories de Thermodynamique et
Physico-Chimie
ENSEEG, BP75
38402 St. Martin d'Heres FRANCE

Dr. Elisabeth Blanquet
LTPCM-ENSEEG
1130 re de la piscine
38402 Saint Martine d'heres Cedex
FRANCE

Dr. Stephanie Watts Butler
Manager, Advanced Process Control
Texas Instruments, Inc.
P.O. Box 655012, MS 944
Dallas TX 75243

Prof. Timothy Cale
Rensselaer Polytechnic Inst.
Dept of CE Ricketts Rm 131
110 8th St.
Troy, NY 12180

Prof. Mark A. Capelli
Dept. of Mechanical Engineering
Stanford University
Building 500
Stanford CA 94305-1901

Prof. Jan-Otto Carlsson
Uppsala University
Chemistry Department
Box 31
S-75121 Uppsala Sweden

Prof. Robert F. Davis
Dept. of Materials Science & Engineering
North Carolina State University
229 Riddick Laboratories
Raleigh NC 27695

Prof. Seshu B Desu
Dept. of Materials Science & Engineering
Virginia Polytechnic Institute
213 Holden Hall
Blacksburg VA 24061-0140

Prof. Demetre J. Economou
Dept. of Chemical Engineering
University of Houston
Houston TX 77204-479

Prof. James Edgar
Department of Chemical Engineering
Kansas State University
Manhattan Kansas 66506-5102

Prof. Alexandre Ern
CERMICS, ENPC
6 et 8, avenue Blasise Pascal
77455 Marne la Vallee cedex 2 FRANCE

Prof. Dr. Ronald A. Fischer
Lehrstuhl fur Anorganische Chemie II
Ruhr-Universitat Bochum
D-44780 Bochum GERMANY

Prof. Ellen R. Fisher
Dept. of Chemistry
Colorado State University
Fort Collins CO 80523-1872

Prof. Arthur Fontijn
Dept. of Chemical Engineering
Rensselaer Polytechnical Institute
110 8th Street
Troy NY 1210-3590

Prof. Steven M. George
Department of Chemistry
University of Colorado
Boulder CO 90309

Prof. David G. Goodwin
Dept. of Mechanical Engineering &
Applied Sciences
California Institute of Technology
Mail Code 104-44
Pasadena CA 91125

Prof. Mark S. Gordon
Dept. of Chemistry
Iowa State University
Spedding Hall 201
Ames IA 50011

Professor Roy G. Gordon
Department of Chemistry
Harvard University
12 Oxford Street
Cambridge MA 02138

Prof. Peter Hess
Institut fur Physikalische Chemie
Heidelberg University
Im Neuenheimer Feld 253
69120 Heidelberg Germany

Prof. Robert F. Hicks
Dept. of Chemical Engineering
University of California
5531 Boelter Hall
Los Angeles CA 90095-1592

Prof. Michael L. Hitchman
Dept. of Pure and Applied Chemistry
University of Strathclyde
295 Cathedral Street
Glasgow G1 1XL United Kingdom

Dr. Frances A. Houle
Science & Technology for Storage
Research Division
IBM Almaden Research Center
San Jose CA 95120-6699

Prof. Klaus Jensen
Dept. of Chemical Engineering
Massachusetts Institute of Technology
Room 66-66
Cambridge MA 02139

Prof. Stanislawa Jonas
Dept. of Ceramics
University of Mining & Metallurgy
Mickiewicza Street 30
30-059 Cracow POLAND

Dr. Lev Kadinski
Lehrstuhl fur Stromungsmechanik
Friedrich-Alexander-Universitat
Cauerstrasse 4
D-91058 Erlangen Germany

Prof. Keith King
Dept. of Mechanical Engineering
University of Adelaide
Adelaide, SA Australia 5005

Prof. H. Komiyama
Dept. of Chemical Engineering
University of Tokyo
Hongo 7, Bunkyo-ku
Tokyo 113 Japan

Dr. F. Langlais
Laboratoire des Composites
Thermostructuraux
Domaine Universitaire
33600 Pessac France

Dr. Woo Y. Lee
Stevens Institute of Technology
Dept. of Materials Science
Hoboken NJ 07030

Prof. M.C. Lin
Dept. of Chemistry
Emory University
Atlanta GA 30322

Prof. Dimitrios Maroudas
Dept. of Mechanical Engineering
University of California, Santa Barbara
Santa Barbara CA 93106-5080

Prof. Paul Marshall
Dept. of Chemistry
University of North Texas
P.O. Box 5068
Denton TX 76203-5068

Prof. Philip W. Morrison, Jr.
Dept. of Chemical Engineering
Case Western Reserve University
10900 Euclid Avenue
Cleveland OH 44106-7217

Prof. Triantafillos J. Mountziaris
Chemical Engineering Dept.
SUNY Buffalo
Buffalo, NY 14260

Dr. Roger Naslain
Laboratoire des Composites
Thermostructuraux
Domaine Universitaire
33600 Pessac FRANCE

Prof. Martyn E. Pemble
Dept. of Chemistry
University of Salford
Salford M5 5WT
United Kingdom

Dr. Michel Pons
Laboratoire de Thermodynamique et
Physio- Chimie
Institut National Polytechnique de Grenoble
ENSEEG
3802 Saint-Martin-D'Heres Cedex France

Prof. Daniel E. Rosner
Chemical Engineering Dept.
Yale University
P.O. Box 2159, Yale Station
New Haven CT 06520-2159

Prof. Douglas K. Russell
The University of Auckland
Science Building
Auckland New Zealand

Prof. H. Bernard Schlegel
Dept. of Chemistry
Wayne State University
Room 365
Detroit MI 48202

Dr. Y. Shimogaki
Univ. of Tokyo
Dept of Metal & Metallurgy
7-3-1 Hongo Bunkyo-ku
Tokyo 113-8656
JAPAN

Prof. Stratis V. Sotirchos
Dept. of Chemical Engineering
University of Rochester
Rochester NY 1467-0166

Dr. Gerald B. Stringfellow
Dean's Office
College of Engineering
University of Utah
1495 E. 100 S. Room 214
Salt Lake City UT 84112-1114

Prof. Francis Teyssandier
CNRS/IMP, UP 8521
Universite, Avenue de Villeneuve
6860 Perpignan Cedex FRANCE

Prof. Stan Veprek
Institute for Inorganic Materials
Technical University of Munich
Lichtenbergstrasse 4
D-85747 Garching Germany

Prof. Robin Walsh
Dept. of Chemistry
University of Reading
Whiteknights
Reading RG6 2AD, England

Prof. Dr. Jurgen Wolfrum
Physikalisch-Chemisches Institut
Ruprecht-Karls-Universitat Heidelberg
Im Neuenheimer Feld 253
69120 Heidelberg Germany

Dr. H. F. Calcote
Director of Research
Chemlon, Inc.
P.O. Box 12
Princeton NJ 08542

Dr. Jitendra S. Goela
Morton Advanced Materials
185 New Boston Street
Woburn MA 01801-6278

Dr. Illan Golecki
Allied Signal, Inc.
101 Columbia Road
Morristown NJ 07962

Dr. Stephen J. Harris
Physical Chemistry Department
GM Research & Development
30500 Mound Road 1-6
Warren MI 48090-9055

Dr. Matthew D. Healy
J.C. Schumacher
1969 Palomar Oaks Way
Carlsbad CA 92009

Dr. Volkmar Hopfe
Dept. Thin Film Technology
Fraunhofer Institute of Material &
Beam Technology
WinterbergstraBe 28
D-01277 Dresden Germany

Dr. Robert Jackson
Novellus Systems, Inc.
81 Vista Montana
San Jose CA 95134

Dr. Jiong-Ping Lu
Texas Instruments, Inc.
13536 N. Central Expressway
Dallas TX 75243

Dr. Francis Maury
Laboratoire des Materiaux
Institut National Polytechnique
118, Route de Narbonne
31077 Toulouse Cedex 4 FRANCE

Dr. Richard J. McCurdy
Pilkington LOF
20th & Center Streets
Ottawa IL 61350

Dr. Meyya Meyyappan
NASA Ames Research Center
Mailstop 229-3
Moffet Field CA 94035

Dr. David Roberts
J.C. Schumacher
1969 Palomar Oaks Way
Carlsbad CA 92009

Dr. John Samuels
Semiconductor Equipment Group
Watkins-JohnsonCo.
440 Kings Village Road, Building 5
Scotts Valley CA 95066-4081

Dr. Michelle T. Schulberg
Novellus Systems Inc.
3970 North First Street
San Jose CA 95134

Dr. David Sheel
Pilkington Technology Management Ltd
Group Research Pilkington Tech Centre
Hall Lane Lathom Ormskirk
Lancashire, England

Dr. Andrew Sherman
Ultranet
12173 Montague Street
Pacoima CA 91331

Dr. Bruce H. Weiller
Mechanics & Materials Technology Center
Aerospace Corporation
P. O. Box 92957
Los Angeles CA 90009-2957

1	MS0601	W. G. Breiland, 1126
1	MS0601	M. E. Coltrin, 1126
1	MS0601	P. Ho, 1126
1	MS9052	M. D. Allendorf, 8361
1	MS9052	D. R. Hardesty, 8361
3	MS9052	A. H. McDaniel, 8361
3	MS9018	Central Technical Files, 8940-2
1	MS 0899	Technical Library, 4916
1	MS 9021	Technical Communications Department, 8528/ Technical Library, MS 0899, 4916
1	MS 9021	Technical Communications Department, 8528 For DOE/OSTI